Global NEST Journal, Vol 27, No X, pp 1-12

Performance evaluation of CMIP6 models for precipitation simulation and prediction of future extreme precipitation in China

Meifang Ren[1,2], Rui Zhang[3,4]* and Fang Yuan[2]
[1]Beijing Key Laboratory of Urban Hydrological Cycle and Sponge City Technology, Beijing 100875, China
[2]China Academy of Urban Planning & Design, Beijing 100044, China
[3]School of Emergency Technology and Management, North China Institute of Science and Technology, 065201, China
[4]Multi-scene water chain accident wisdom emergency technology innovation center of Hebei, 065201, China
Received: 09/06/2025, Accepted: 03/12/2025, Available online: 08/12/2025
*to whom all correspondence should be addressed: e-mail: rzhang1808@163.com
https://doi.org/10.30955/gnj.07738

Graphical abstract

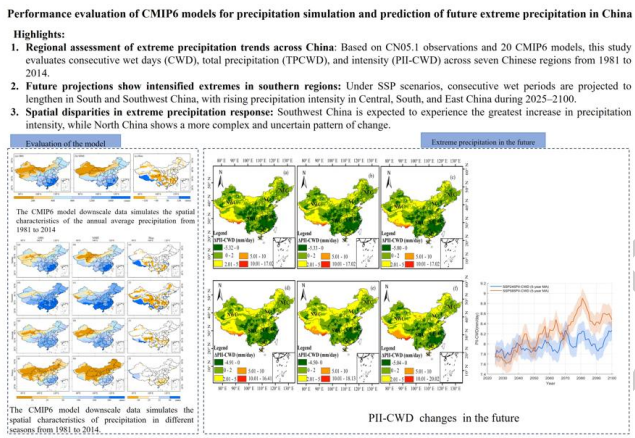

Abstract

Using the CN05.1 dataset, evaluated the simulation abilities about 20 CMIP 6 models and investigated the changes of numbers of extreme precipitation indices which related to the consecutive wet days in seven regions of China. The variations between the future (2025-2100) and the history (1981-2014) have been investigated according to the ΔPII-CWD indices and the relationships between these indices and the R95p extreme precipitation index were analyzed under two shared socioeconomic pathway scenarios. Results showed that the multi-model ensemble (MME) results better reproduce the spatial distribution characteristics of annual average precipitation in China. The maximum consecutive wet days (CWD) were projected to be substantially longer in South China and Southwest China in the historical periods, especially in Guangdong, the Sichuan Basin, and the other areas, exceeding 10d, and the precipitation intensity index (PII-CWD) were predicted to be higher in Central China, South China, and East China, with PII-CWD exceeding 10 mm/day. The multi-model ensemble mean predicted more severe and frequent extreme precipitation events during 2025–2100, and the greatest changes were projected to occur in Southwest China around 2070 and 2080. Overall, the projected pattern of extreme precipitation in North China is complex, whereas South China is expected to experience more frequent and intense extreme precipitation events in the future.

Keywords: extreme precipitation; Coupled Model Intercomparison Project Phase 6 (CMIP6); consecutive wet days; climate change; future projection

1. Introduction

One of the most profound consequences of global warming is the worldwide redistribution of precipitation, which includes changes in the spatial and temporal trends of precipitation, as well as variations in the intensity and duration of precipitation extremes (Allan *et al.* 2008; Papalexiou *et al.* 2019). The sixth assessment report of the Intergovernmental Panel on Climate Change highlighted that with every 1 °C increase in global temperature in the future, the intensity of extreme daily precipitation events is projected to rise by 7% (IPCC 2021). Previous studied have shown that climate change will intensify the global and regional water cycles, the frequency and intensify of the extreme precipitation events have increased significantly, which have substantial effects on human society and natural ecosystems (Mishra *et al.* 2010; Croitoru *et al.* 2016; Brown *et al.* 2008). Urban flooding is one of the severe natural disasters in China, investigation the changes in extreme precipitation and their impacts under the climate change have an important practical significance for regional flood control and disaster mitigation in China.

The Coupled Model Intercomparison Project Phase 6 (CMIP6) represents the latest version from the CMIP organization, providing new opportunities for projecting climate variables by integrating advanced and revised dynamic process parameter methods (O'Neill *et al.* 2014), along with new emission scenarios. The emission pathways in CMIP6 include scenarios ranging from low emissions with sustainable development (SSP1-2.6), moderate emissions with balanced development (SSP2-4.5), higher emissions with unbalanced development (SSP3-7.0), to high emissions relying on fossil fuels (SSP5-

8.5), simulating future climate changes under different socio-economic conditions. Recent studies have utilized CMIP6 models to assess and predict climate extremes (Jiang *et al.* 2020; Chen *et al.* 2020). For example, using CMIP6 data to estimate extreme precipitation in China, Xiang *et al.* (2021) found that regional extreme precipitation is expected to increase substantially during 2021–2100. Chen *et al.* (2020) demonstrated that the CMIP6 multi-model ensemble (MME) mean provides a comprehensive improvement in modeling global climate averages and extremes, characterized by relatively low model uncertainty. In China, both temperature and precipitation are projected to increase by the end of the 21st century, with the largest increase in annual precipitation expected in northern and western regions (Yang *et al.* 2021). The ability of climate models to simulate extreme rainfall is generally considered to have improved, as evidenced by numerous global studies. However, in regions with complex topography, improvements have been limited relative to the performance of CMIP5 models (Lun *et al.* 2021). Moreover, these studies primarily focused on the performance of CMIP6 models in terms of either mean annual precipitation or individual extreme precipitation indices.

The consecutive wet days (CWD) is an important climate indicator for assessing extreme precipitation events (Huang *et al.* 2017). which means the number of days when the daily precipitation ≥1mm. The consecutive extreme precipitation events, including persistent heavy rainfall and prolonged downpours, are major triggers for floods, landslides, and mudslides, for example, the consecutive heavy rainfall lasting 5 days is far more likely to trigger catastrophic floods than a single day of heavy rain. Studies have shown that long-duration rainy days, which are more likely to trigger flooding events due to high rainfall totals (Li *et al.* 2017; Wu *et al.*,2019), also lead to associated secondary and spin-off meteorological hazards (Huang *et al.* 2017; Wu *et al.* 2019). Therefore, analyzing the changes in CWD and their causes is beneficial for both climate disaster risk management and climate change mitigation and adaptation (Li *et al.* 2012).

Previous studies of CWD have primarily focused on analyzing the temporal trend and spatial distributions at various scales, including global (Singh *et al.* 2014), continental (Alexander *et al.* 2016), national (Roque-Malo *et al.* 2017), and regional levels (Shi *et al.* 2018), and have identified generally inconsistent characteristics in CWD. Li *et al.* (2019) studied the extreme precipitation index in China for the period 1961–2017 and found that CWD showed a declining trend. Cai *et al.* (2024) studied extreme precipitation in Shanxi Province, China, for the period 1972–2020. They found that CWD gradually declined from the central part of the study area to the eastern and western parts of the province, with a decreasing rate of −0.1 days per decade. CWD has been found to have stronger correlation with flash flood events compared to other indices (Acquaotta *et al.* 2019), and some studies have examined the trends in CWD and their impact on flood events. For example, in the Colombian Andes, flood events have been linked to extreme rainfall as well as changes in CWD and consecutive dry days (Ávila *et al.* 2019). Overall, research on CWD and its relationship with floods has provided valuable insights into the potential impacts of changing precipitation patterns on flood events. Monitoring CWD and other extreme precipitation indices allows researchers to better understand and prepare for the increasing risks of flooding in a changing climate (Shruti *et al.* 2020). Despite the significance of CWD in extreme precipitation analysis, research on in-depth analysis of the variation trends of the CWD indices in China across historical and future periods remain relatively limited.

The objectives of this study were to analyze the spatiotemporal characteristics of CWD from 1981 to 2014 and to project future changes in total precipitation, CWD precipitation intensity, and R95p. To achieve this, we utilized daily precipitation data from the CN05.1 observational dataset and the regional climate models under the SSP245 and SSP585 scenarios. The analysis was conducted using extreme precipitation indices defined by the Expert Team on Climate Change Detection and Indices (ETCCDI). We performed regional climate model projections for the near-future (2025–2050), mid-future (2051–2075), and far-future (2076–2100) periods relative to the historical baseline (1981–2014). Furthermore, China was divided into seven subregions according to climatic zoning principles to facilitate a detailed spatial assessment of extreme precipitation changes. The primary goal was to provide insights for the mitigation and prevention of flood disasters, and to support water resources management in various regions of China.

2. Materials and Methods

2.1. Data

This study used the CN05.1 grid dataset, which is interpolated from observational data recorded at over 2400 ground-based meteorological stations in China. This dataset is provided by the Climate Change Research Center, Chinese Academy of Sciences (https://ccrc.iap.ac.cn/resource/detail?id=228). It was subjected to strict quality control and homogenization checks before release. This dataset, which is used widely in precipitation research in China, has spatial resolution of 0.25° (approximately 25 km × 25 km). The historical data for the years 1981–2014 were used in this study.

The first version of the NASA Earth Exchange Global Daily Downscaled Projections (NEX-GDDP) dataset, NEX-GDDP-CMIP5, was released in 2015 and has been widely applied in studies of climate change impacts at both global and local scales (Kumar *et al.* 2020; Zhang *et al.* 2019; Zeng *et al.* 2019). The latest version, NEX-GDDP-CMIP6, includes downscaled data from 35 models spanning 1950 to 2100 (covering both historical and future periods) based on CMIP6 model outputs (Thrasher *et al.* 2022; Zhang *et al.* 2024). The bias correction and spatial disaggregation (BCSD) method was applied to the NEX-GDDP-CMIP6 dataset to uniformly downscale the

original CMIP6 output to daily data with a spatial resolution of 0.25°. The NEX-GDDP-CMIP6 dataset was calibrated using a global meteorological forcing dataset, which incorporated both reanalysis data and observations (Thrasher *et al.* 2022; Sheffield *et al.* 2006).

Considering the consistency of scenarios and data availability for the required time periods, we selected 20 downscaled model simulations (**Table 1**) that provide complete daily precipitation data spanning both the historical baseline (1981-2014) and future periods (2025-2100) under two SSP-RCP scenarios (SSP245 and SSP585) across China. These criteria ensure comprehensive coverage for predicting future extreme precipitation indices while maintaining scenario consistency. Detailed information and documentation on the NEX-GDDP-CMIP6 dataset are available online at https://www.nccs.nasa.gov/services/data-collections/land-based-products/nex-gddp-cmip6.

Table 1. CMIP6 models included in the NEX-GDDP-CMIP6 dataset

No.	Names	Modeling center (or group)
1	ACCESS-CM2	Commonwealth Scientific and Industrial Research Organization
2	ACCESS-ESM1-5	Climate System Science (ARCCSS), Australia
3	CanESM5	Canadian Centre for Climate Modeling and Analysis (CCCma)
4	CMCC-CM2-SR5	Fondazione Centro Euro-Mediterraneo sui Cambiamenti Climatici (CMCC), Italy
5	CMCC-ESM2	Fondazione Centro Euro-Mediterraneo sui Cambiamenti Climatici (CMCC), Italy
6	CNRM-CM6-1	Centre National de Recherches Meteorologiques (CNRM) and Centre
	CNRM-ESM2-1	Scientifique (CERFACS), France
8	EC-Earth3	A European community Earth-System Model (EC-Earth-consortium)
9	EC-Earth3-Veg-LR	
10	FGOALS-g3	Chinese Academy of Sciences (CAS), China
11	GFDL-CM4(gr1)	National Oceanic and Atmospheric Administration, Geophysical Fluid Dynamics Laboratory (NOAA-GFDL), USA
12	GFDL-CM4(gr2)	National Oceanic and Atmospheric Administration, Geophysical Fluid Dynamics Laboratory (NOAA-GFDL), USA
13	GFDL-ESM4	National Oceanic and Atmospheric Administration, Geophysical Fluid Dynamics Laboratory (NOAA-GFDL), USA
14	GISS-E2-1-G	Goddard Institute for Space Studies (NASA-GISS), USA
15	INM-CM4-8	Institute for Numerical Mathematics (INM), Russian Academy of Science, Russia
16	INM-CM5-0	Institute for Numerical Mathematics (INM), Russian Academy of Science, Russia
17	IPSL-CM6A-LR	Institut Pierre Simon Laplace (IPSL), France
18	MIROC6	Japan Agency for Marine-Earth Science and Technology, Atmosphere and Ocean Research Institute, The University of Tokyo, National In-sti tute for Environmental Studies, and RIKEN Center for Computa-tional Science, Japan
19	MIROC-ES2L	Japan Agency for Marine-Earth Science and Technology, Atmosphere and Ocean Research Institute, The University of Tokyo, National Institute for Environmental Studies, and RIKEN Center for Computational Science, Japan
20	MPI-ESM1-2-HR	Max Planck Institute for Meteorology (MPI-M), Germany

2.2. Methods

This section provides a detailed description of the specific methods used in this study, including evaluation metrics, the selection and definition of extreme precipitation indices, and the spatial analysis method employed.

2.2.1. Evaluation metrics

To evaluate model performance and analyze results, we used the correlation coefficient (R), standard deviation (SD), and root mean square error (RMSE). These metrics are widely adopted in climate studies to quantify the accuracy and variability of model outputs relative to observations. The calculation procedures followed the standard methodologies as detailed in reference (Zhan *et al.* 2017).

2.2.2. Extreme precipitation indices

Extreme precipitation indices were selected based on the recommendations of the Expert Team on Climate Change Detection and Indices (ETCCDI), which have been widely used in climate extreme analyses (Dong *et al.* 2015). To avoid redundancy among strongly correlated indices, we focused on two core indices indicative of extreme rainfall: R95p (annual total precipitation exceeding the 95th percentile) and CWD (maximum consecutive wet days). These indices effectively capture the intensity and persistence of precipitation extremes.

To further investigate the characteristics of sustained rainfall events, we introduced three derived indices:

TPCWD: Total precipitation during consecutive wet days, reflecting the cumulative rainfall amount in prolonged wet periods.

PII-CWD: Precipitation intensity during consecutive wet days, calculated as TPCWD divided by CWD. This index helps distinguish between events with high precipitation accumulation due to longer duration versus higher intensity.

R1 and R2: Ratios quantifying the relationship between extreme precipitation days (R95p) and consecutive wet days (CWD). R1 represents the proportion of extreme precipitation days within wet periods, while R2 indicates the contribution of extreme precipitation to total wet-period rainfall. These ratios provide insights into the internal structure of wet spells and the concentration of extreme rainfall. All indices are listed in **Table 2**.

The selection of these indices was motivated by the need to analyze not only the frequency and amount of extreme precipitation but also its behavior within extended wet periods, which is critical for understanding flood risks and rainfall persistence under climate change.

To analyze the change rates of PII-CWD in different regions of China over various time scales relative to historical periods under different scenarios, the future period prediction was divided into three phases: 2025–2050 2051–2075, and 2076–2100. To clarify the regional characteristics of extreme indices, China was further subdivided according to administrative geographical zoning into seven regions: Southwest China (SWC), Northwest China (NWC), North China (NC), South China (SC), Central China (CC), East China (EC), and Northeast China (NEC) (Peng *et al.* 2017).

Table 2. Extreme precipitation indices.

Index	Definition	Unit
R95p	Annual total precipitation when daily precipitation > 95th percentile	mm
CWD	Maximum number of consecutive wet days (i.e. when R ≥ 1 mm)	day
TPCWD	Total precipitation of CWD	mm
PII-CWD	The ratio of TPCWD to CWD	mm/day
R1	The ratio of days of R95p to CWD	/
R2	The ratio of R95p to the precipitation of CWD	/

Table 3. Classification of the Hurst index.

Level	H Value Range	Persistence Strength	Level	H Value Range	Anti-Persistence Strength
1	0.50<H≤0.55	very weak	-1	0.45≤H<0.50	very weak
2	0.55<H≤0.65	relatively weak	-2	0.35≤H<0.45	relatively weak
3	0.65<H≤0.75	relatively strong	-3	0.25≤H<0.35	relatively strong
4	0.75<H≤0.80	Strong	-4	0.20≤H<0.25	strong
5	0.80<H≤1.00	very strong	-5	0≤H<0.20	very strong

2.2.3. Getis-Ord Gi spatial hotspot analysis method*

The Getis-Ord Gi* spatial hotspot analysis is a method used to identify the distribution of hotspots and cold spots of a study object within a local spatial context (Getis *et al.* 1992). In this study, it was employed to identify spatially significant clusters of high and low values of PII-CWD. This method is effective for detecting local spatial patterns and has been widely used in geographical and climate research. The calculation formula is expressed as follows:

$$G_i^* = \frac{\sum_j \omega_{ij} x_j - \overline{X} \sum_j \omega_{ij}}{S\sqrt{\frac{\left[n\sum_j \omega_{ij}^2 - (\sum_j \omega_{ij})^2\right]}{n-1}}} \quad (1)$$

where ωij is the spatial weight matrix representing the spatial weight between regions i and j, x_j is the value of variable *x* in region j, $\overline{X}$ is the global mean of variable *x*, S is the standard deviation of variable *x*, and n is the total number of regions.

Hotspots represent regions with high Z-scores and low p-values (typically <0.05), indicating statistically significant high-value clusters. Cold spots represent regions with low Z-scores and low p-values, indicating statistically significant low-value clusters. Nonsignificant areas area regions with high p-values, indicating no statistically significant clustering of high or low values.

2.2.4. Hurst index

To predict the trend of future extreme precipitation events, this study utilized the R/S analysis method to calculate the Hurst index (H-value) (Mandelbrot *et al.* 1968). Based on the magnitude of the daily values, the sustainability and anti-sustainability of future trends can be determined. The intensity grading is summarized as follows: when 0 < H < 0.5, the future trend of change is opposite to that of the past; when 0.5 < H < 1, the future trend of change is consistent with that of the past; and when H = 0.5, the future trend of change exhibits no long-term memory and represents a random walk. If the H-value is close to 1, the persistence of the trend is stronger; if the H-value is close to 0, the anti-persistence of the trend is stronger. The specific strength grading detailed are listed in **Table 3.**

3. Results

3.1. Evaluation of simulation ability of models

3.1.1. Evaluation of simulation capability for spatial climate state characteristics

To evaluate the models, data from the historical period (1981–2014) were selected for comprehensive analysis.

To assess the capability of the models in simulating average annual precipitation in China using downscaled data from the NEX-GDDP-CMIP6 dataset, this study compared observed data, model outputs, and their differences (**Figure 1**). Both observations and the MME mean show significant spatial heterogeneity in multiyear

average precipitation across China, declining from over 1600 mm in SEC to less than 200 mm in NWC (**Figure 1a, b**). The MME mean accurately replicates the spatial distribution of observed annual average precipitation in China. However, it underestimates average annual precipitation in most regions of China (by >150 mm), primarily in SC and NC, while significantly overestimating it in Tibet (**Figure 1c**). These discrepancies highlight challenges in simulating local climatic influences such as orographic precipitation and high-elevation processes, particularly due to the complex topography and sparse observational data in Tibet. The MME effectively captures the overall spatial pattern of precipitation distribution, particularly the gradient from the SEC to the NWC, consistent with other related studies (Ma *et al.* 2022; Wu *et al.* 2023).

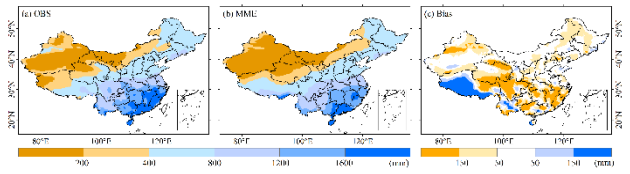

Figure 1. Spatial characteristics of annual average precipitation from 1981–2014

3.1.2. Evaluation of simulation capability for spatial climatic state characteristics of seasonal precipitation

This study further evaluated the ability of downscaled CMIP6 model data to accurately replicate seasonal precipitation patterns in China (**Figure 2**). The first to fourth rows of the **Figure 2** represent the four seasons, with the leftmost column representing the observed values, the middle column representing the MME, and the rightmost column representing the bias of the MME and the observed values. Observational data show a gradient in average spring precipitation, with high values in SEC (> 500 mm) and low values in NWC (<20 mm) (**Figure 2a**). The spring model ensemble's spatial distribution is similar to observed data, but the range of low annual precipitation values (<10 mm) in NWC is larger (**Figure 2b**). Differences between the MME mean and observations are minor in the northern region (±25 mm) and most southern areas (approximately 50 mm), with anomalies around 50 mm more prevalent in the hinterland and southern parts of the Qinghai–Tibet Plateau.

In summer, observed precipitation is highest, with the highest values (>500 mm) in SC and SEC, and the lowest values (<50 mm) in NWC (**Figure 2d**). The downscaled CMIP6 data capture these patterns but overestimate low-value precipitation areas in NWC and show anomalies in the hinterland and southern parts of the Qinghai–Tibet Plateau. The MME underestimates precipitation in most regions but overestimates it on the Qinghai-Tibet plateau (**Figure 2f**). While the MME captures the general spatial patterns, there are discrepancies in extreme dry and wet areas. These findings highlight both the strengths and limitations of the models in replicating regional precipitation patterns in China, underscoring the need for further refinement to improve accuracy in specific areas.

In autumn, both observations and MME show high precipitation (>200 mm) in SEC and low precipitation (<20 mm) in NWC (**Figure 2g, h**). Errors are minor, with slight overestimation in Chengdu (**Figure 2i**), indicating better performances in autumn, but with localized biases.

In winter, precipitation is lower in most regiones except the SEC (100–500 mm). The MME reflects this pattern but shows more extensive reduction in NC with levels <10 mm (**Figure 2j, k**). The MME slightly underestimates precipitation in SEC and overestimates it along the western periphery (25-50 mm) (**Figure 2l**). It indicates that while the MME effectively captures the broad spatial trends of winter precipitation, it faces challenges in accurately representing finer-scale details, particularly in the northern and peripheral regions.

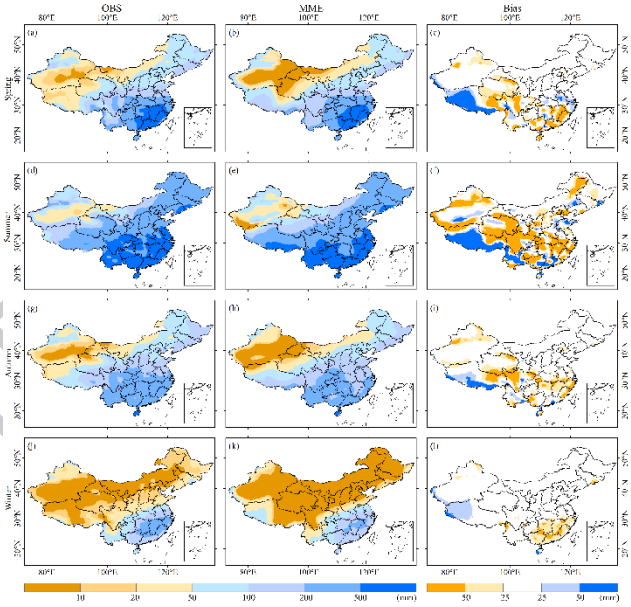

Figure 2. Spatial characteristics of precipitation in different seasons from 1981 to 2014

3.1.3. Spatial evaluation indices for precipitation

To further assess the spatial characteristics of average annual precipitation across various models in relation to China, this study used Taylor plots to evaluate these characteristics.

According to **Figure 3a**, the Taylor plot reveals several key metrics highlighting the performance of the CMIP6 downscaling models in simulating annual precipitation. The spatial correlation coefficient (R) between the modeled and observational values at the grid points ranges from 0.9 to 0.95, indicating a high correlation. This high correlation suggests that the models successfully capture the spatial patterns of annual precipitation observed across China.

The standardized standard deviation of the simulated annual precipitation is approximately 0.9, indicating that the model simulations have slightly smaller spatial fluctuation amplitudes than the observed values. The central root mean square error of the simulated annual

average precipitation for each model is about 0.4, indicating small errors.

The Taylor plot also illustrates the performance of the models in different seasons: spring, summer, autumn, and winter. These seasonal assessments are crucial as they provide insights into how well the models perform under various climatic conditions throughout the year. From the seasonal assessments, the MME shows the most consistent performance across all seasons. The minor differences in these three indicators among the models in the Taylor plot suggest that both the individual models and the ensemble can effectively simulate the annual average climatic state of precipitation in China.

Figure 3b–e shows that the seasonal spatial R between the modeled and the observational values at the grid points exceeds 0.9, except in summer, where it is slightly below 0.9. This indicates a high correlation between the simulated and observed patterns of seasonal precipitation. The standardized standard deviation of the simulated seasonal precipitation is slightly below 1, suggesting reduced spatial fluctuation compared to the observed values. The root mean square error for each model is approximately 0.4, indicating minimal error. The small variations among these indicators suggest that both the individual models and the ensemble can effectively simulate the seasonal precipitation patterns in China, consistent with previous studies (Tian *et al.* 2021).

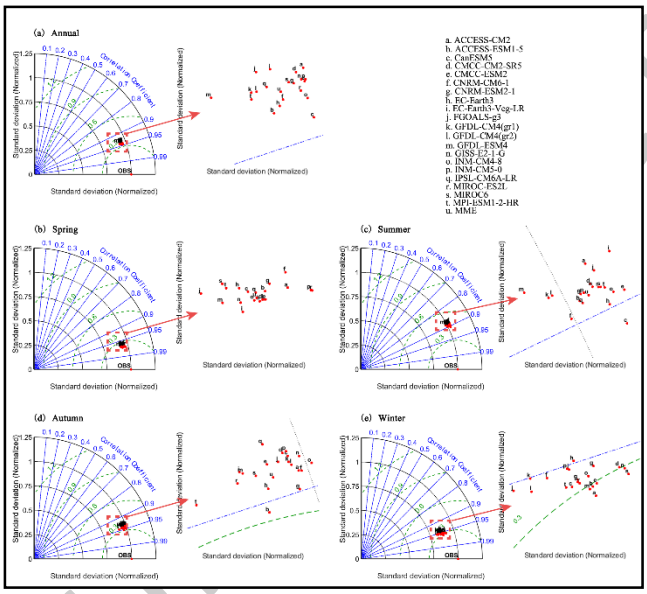

Figure 3. Taylor plot of average annual and seasonal precipitation simulated by the CMIP6 downscaling models. The radial scale shows R, the y-axis represents the ratio of the standard deviation (STD) between the simulated and observed values, and the green semicircles indicate the root mean square error

3.2. Analysis of extreme precipitation indices

To further analyze the future changes in extreme precipitation indices, we examined the temporal and spatial variations of these indices based on the MME. This approach provided a comprehensive understanding of how extreme precipitation events might evolve under different climate change scenarios.

3.2.1. Analysis of extreme precipitation indicators in historical periods

Figure 4 shows the spatial distribution of the maximum number of consecutive wet days (CWD), the total precipitation of CWD (TPCWD), the ratio of TPCWD TO CWD (PII-CWD) across China from 1981 to 2014, highlighting regional differences in extreme precipitation events. In SC and SWC, CWD is significantly longer (**Figure 4a**). Notably, Guangdong and the Sichuan provinces exhibit CWD values exceeding 10 d, indicating a higher number of consecutive precipitation days and an increased risk of long-term precipitation events, consistent with other studies (Tian *et al.* 2021) [50]. These regions experience longer duration precipitation, correlating with increased flood risk. In Xinjiang, higher CWD values are observed in the Tianshan Mountains, one of the wettest areas in Xinjiang.

Figure 4b shows that TPCWD in SC is markedly higher than in other regions, with an average value exceeding 100 mm. This indicates a higher propensity for flooding, consistent with the findings of Chen *et al.* (2023), who reported that extended CWD periods often precede significant flooding events owing to the accumulation of precipitation over consecutive days. The highest CWD values are in SWC, particularly in the southeastern Tibet. However, despite high CWD values, TPCWD values are not as high as in SC, indicating relatively low daily rainfall in SWC.

Figure 4c shows the distribution of PII-CWD, with high values in CC, SC, and EC, where PII-CWD exceeds 10 mm/day. This distribution resembles the segmentation of the "Hu Huanyong Line," with lower values on the western side and higher values on the eastern side.

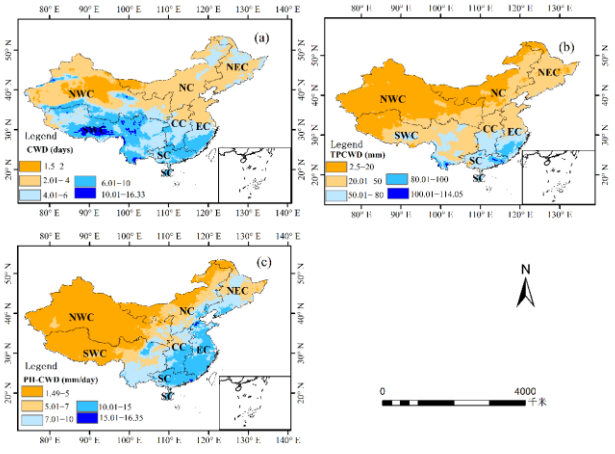

Figure 4. Spatial distribution of multiyear averages of (a) CWD, (b) TPCWD, and (c) PII-CWD from 1981 to 2014

3.2.2. Spatial variation of ΔPII-CWD in the future

PII-CWD is crucial for understanding extreme precipitation events and their potential impacts. This study investigated the spatiotemporal changes in PII-CWD compared to historical periods under the SSP245 and SSP585 scenarios, referred to as ΔPII-CWD. The ΔPII-CWD was calculated for three future periods: 2025–2050, 2051–2075, and 2076–2100. A *t*-test conducted on the ΔPII-CWD for various

periods under both scenarios showed statistically significant results ($p<0.05$).

Figure 5 illustrates substantial regional differences in ΔPII-CWD under these scenarios. Under the SSP245 scenario, SWC exhibits the largest increase in ΔPII-CWD from 2025 to 2050, with values exceeding 5 mm/day and reaching over 10 mm/day in some areas, indicating a heightened risk of extreme precipitation and flooding This trend continues and intensifies in subsequent periods, likely due to increased monsoon activity and higher humidity (Lin *et al.* 2018; Zhang *et al.* 2008). Conversely, EC, CC, and SC show reductions in ΔPII-CWD (−5.32 to 0 mm/day), suggesting reduced risk of wet days but potentially higher drought risk Under the SSP585 scenario, the initial increase in ΔPII-CWD (2025–2050) is more pronounced than under the SSP245 scenario, with a notable expansion in areas experiencing increased precipitation intensity by 2076–2100, especially in SWC and northern NC.

To provide a concise synthesis of these complex spatial patterns and facilitate comparison across regions and scenarios, the principal characteristics of ΔPII-CWD changes are summarized in **Table 4**. The table clearly highlights the stark contrast between the strongly increasing trends in SWC and the declining trends in eastern and central regions. This highlights the critical impact of high emissions on extreme weather events (Chen *et al.* 2019; Kharin *et al.* 2013). The consistency of these trends over time underscores the urgency of reducing greenhouse gas emissions to mitigate future extreme precipitation risks and the necessity for adaptive measures in high-risk regions. These findings align with global studies on extreme precipitation, emphasizing the need for robust regional planning and international cooperation in climate mitigation efforts (Lin *et al.* 2018; Zhang *et al.* 2008; Kharin *et al.* 2013).

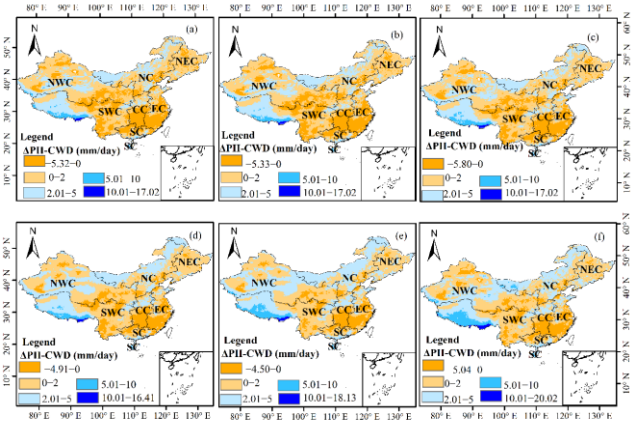

Figure 5. Changes in PII-CWD relative to historical periods under future scenarios: (a)–(c) 2025–2050, 2051–2075, and 2076–2100 under the SSP245 scenario, respectively, and (d)–(f) 2025–2050, 2051–2075, and 2076–2100 under the SSP585 scenario, respectively

Table 4. Summary of projected changes in PII-CWD across Chinese subregions under different scenarios (relative to the historical period)

Region	SSP245 Scenario	SSP585 Scenario	Key Characteristics	
SWC (Southwest)	++ (Marked increase, > 5 mm/day)	+++ (Strong increase, > 10 mm/day)	Largest increase, intensifying with time and higher emissions	
SC (South)	- (Slight decrease)	~0 to + (Stable to slight increase)	Relatively minor changes with higher uncertainty	
NC (North)	~0 (Non-significant change)	+ (Apparent increase, especially in the north)	Increased risk in northern parts under high emissions	
EC (East)	- (Decrease)	- (Decrease)	Decreasing trend under both scenarios	
NWC (Northwest)	+ (Slight increase)	++ (Significant increase)	Low baseline but notable relative increase	
NEC (Northeast)		~0 (Non-significant change)	+ (Slight increase)	Generally weak changes overall
CC (Central)	- (Decrease)	- to ~0 (Decrease to stable)	Predominantly decreasing trend	

3.2.3. Future changes in PII-CWD

Figure 6 shows the five-year moving average of the ratio of the TPCWD to CWD (PII-CWD) under the SSP245 and SSP585 scenarios. Under the SSP245 scenario, PII-CWD exhibits a slight upward trend, indicating that while climate change impacts persist, their volatility and long-term growth remain manageable, reflecting the effectiveness of emission reduction policies (Eyring *et al.* 2016; Riahi *et al.* 2017). Conversely, under the SSP585 scenario, PII-CWD shows a higher growth rate and intensified interannual fluctuations, revealing the complex and nonlinear responses of the climate system to high emissions. The marked expansion of the orange-shaded area indicates increased uncertainty in climate model predictions, attributable to complex feedback mechanisms under high temperature stress, potentially leading to more frequent extreme climate events (Cook *et al.* 2020). These findings underscore the necessity for robust emission reduction strategies and adaptive measures to mitigate the impacts of climate change (Eyring *et al.* 2019).

3.2.4. Trends in R1 and R2 in the future

To further analyze the frequency and intensity of changes in extreme weather, we examined the ratio of TPCWD to

CWD (R1) and the ratio of days of R95p to CWD (R2) across the seven defined regions of China, as shown in **Figures 7 and 8**. The trends in R1 and R2 from 2025 to 2100 under the SSP245 and SSP585 scenarios reveals notable regional differences and an overall upward trend. In SC, R1 peaks around 2070 and 2080 under both scenarios, indicating a substantial increase in R95p events compared to CWD. This indicates that climate change may lead to more frequent and intense precipitation events in areas already prone to such extremes (Zhang *et al.* 2008; Ai *et al.* 2022). NC also shows a sharp upward trend. Under the SSP245 scenario, other regions exhibit relatively stable trend in R1 with minimal fluctuations, indicating more uniform variation in extreme precipitation (Yang *et al.* 2018). In contrast, under the SSP585 scenario, most regions have higher R1 values than under the SSP245 scenario, highlighting more pronounced changes with higher emissions (Cook *et al.* 2020). The width of the confidence intervals varies across regions and periods, especially in e peak years, indicating high prediction uncertainty, likely due to the variability in predicting extreme weather events. The consistent upward trend in extreme precipitation aligns with global climate projections, posing significant challenges for water management and disaster reduction, particularly in high-risk areas such as SC (IPCC 2021).

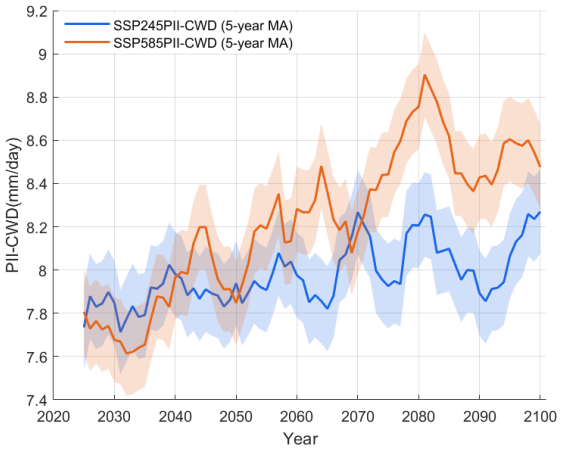

Figure 6. Five-year moving average of PII-CWD under the SSP245 and SSP585 scenarios from 2025 to 2100

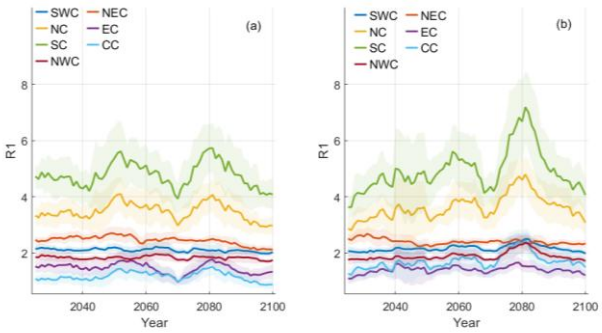

Figure 7. Five-year moving average of R1 under (a) the SSP245 scenario and (b) the SSP585 scenario from 2025 to 2100

Figure 8 illustrates the projected future trend of R2 in different regions of China under the two scenarios. Overall, except in EC and NEC, R2 values are expected to fluctuate with an upward trend under the SSP245 scenario, indicating an increase in the frequency and intensity of R95p events, particularly in CC and SC, where the average ratio exceeds 5. NC and EC exhibit relatively stable changes with minor fluctuations, indicating balanced changes in R95p events and CWD, while SWC and NWC remain stable under both scenarios. Under the SSP585 scenario, R2 in all regions is generally higher than under the SSP245 scenario, indicating a substantial increase in extreme precipitation events under the high-emission pathway. This trend aligns with findings from other studies (Ji *et al.* 2015), which reported an increasing trend in extreme precipitation in SC attributable to global warming. High-emission pathways, as highlighted by Chen *et al.* (2020) and the Intergovernmental Panel on Climate Change (IPCC 2021), enhance the atmosphere's water-holding capacity, leading to more extreme precipitation events. To address these challenges, regions must strengthen water resource management and disaster prevention measures, such as improving drainage systems and water storage facilities, and raise public awareness regarding disaster preparedness (Cai *et al.* 2020).

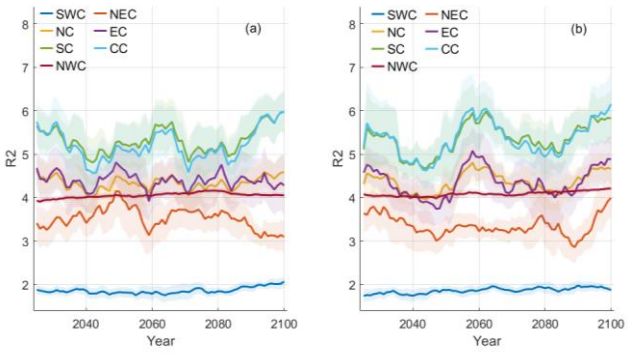

Figure 8. Five-year moving average of R2 under (a) the SSP245 scenario and (b) the SSP585 scenario from 2025 to 2100

4. Discussion

4.1. Spatial patterns and regional mechanisms of ΔPII-CWD

The spatial distribution of the average changes in PII-CWD compared to historical periods (ΔPII-CWD) reveals significant regional disparities under different emission scenarios, shaped by a confluence of climatic, topographic, and anthropogenic factors. Regions such as Hebei Province, Beijing, and Tianjin in NC, ΔPII-CWD is projected to increase over different periods under both scenarios despite limited precipitation, which may be attributed to enhanced moisture convergence due to urbanization and intensified anthropogenic heating, altering local precipitation regimes. Conversely, parts of SC and most of CC show a declining trend, indicating a reduction in average precipitation during CWD. However, the extent of these reduced areas will shrink, indicating that these regions will continue to experience a high incidence of extreme precipitation events and an increasing risk of flooding. This trend underscores the significant challenges posed by climate change, as

frequent and intense extreme precipitation events could threaten socioeconomic stability and infrastructure.

These findings highlight the need for in-depth research on the regional characteristics of climate change to develop effective disaster reduction and adaptation measures. The results demonstrate the diverse spatial patterns of CWD events. It is important to note that the definition of CWD events is based on daily precipitation, which exhibits considerable spatial heterogeneity owing to the influence of natural characteristics and human activities (Tammets and Jaagus 2013; Jiao *et al.* 2015). This results in variation in precipitation duration and differences in TPCWD. Given the high heterogeneity of precipitation and the suddenness of extreme events (Sura 2011), it is crucial to explore the nature of consecutive precipitation events from a spatial perspective to highlight regional differences in wetting duration.

4.2. Persistence and future trends of R1 and R2

The application of the R/S analysis reveals a strong persistence (H > 0.5) in both the ratio of TPCWD to CWD (R1) and the ratio of days of R95p to CWD (R2) across most regions under SSP245 and SSP585 scenarios, indicating that current trends in frequency, intensity, and duration of extreme precipitation are likely to continue (**Tables 5 and 6**). The "strong" and "very strong" persistence levels (H $\geq$ 0.7) under SSP585, particularly in EC, SC, and NC, suggest that higher emission pathways will amplify existing trends, leading to more frequent and intense extreme precipitation events.

Regionally, the weaker persistence in SWC and NWC under SSP245 may be related to the complex interplay between monsoon variability and topographical constraints. However, under higher emissions (SSP585), even these regions exhibit strengthened persistence, indicating a broader and more uniform influence of climate change. These findings align with existing research suggesting an increase in the persistence of weather extremes due to thermodynamic changes and altered atmospheric dynamics. The results emphasize that future climate adaptation strategies must account for prolonged and intensified precipitation extremes, particularly in regions showing high H-values.

Table 5. H-values of R1 and persistence intensity under the SSP245 and SSP585 scenarios from 2025–2100

Region	R1					
	SSP245	Persistence and Anti-Persistence Strength	Level	SSP585	Persistence and Anti-Persistence Strength	Level
SWC	0.63	Relatively Weak	2	0.74	Relatively Strong	3
NEC	0.67	Relatively Strong	3	0.73	Relatively Strong	3
NC	0.71	Relatively Strong	3	0.76	Strong	4
EC	0.69	Relatively Strong	3	0.82	Very Strong	5
SC	0.76	Strong	4	0.78	Strong	4
CC	0.69	Relatively Strong	3	0.74	Relatively Strong	3
NWC	0.61	Relatively Weak	2	0.74	Strong	3

Table 6. H-values of R2 and persistence intensity under the SSP245 and SSP585 scenarios from 2025 to 2100.

Region	R2					
	SSP245	Persistence and Anti-Persistence Strength	Level	SSP585	Persistence and Anti-Persistence Strength	Level
SWC	0.75	Relatively Strong	3	0.69	Relatively Strong	3
NEC	0.69	Relatively Strong	3	0.69	Relatively Strong	3
NC	0.67	Relatively Strong	3	0.73	Relatively Strong	3
EC	0.67	Relatively Strong	3	0.61	Relatively Weak	2
SC	0.65	Relatively Weak	2	0.70	Relatively Strong	3
CC	0.70	Relatively Strong	3	0.72	Relatively Strong	3
NWC	0.78	Strong	4	0.76	Strong	4

4.3. Spatial clustering and regional implications of PII-CWD

To further explore the spatial clustering patterns of PII-CWD and reveal the impacts of climate change on the precipitation distribution, spatial clustering analysis was conducted using the Getis Ord Gi* statistic. This approach helped identify regional risk levels associated with extreme precipitation events across China (**Figure 9**). Hotspot analysis (shown in red) revealed that high PII-CWD values are predominantly concentrated in EC, SC, parts of CC, and the southern periphery of SWC. These areas exhibit significantly elevated precipitation intensity, likely attributable to monsoonal influences, topographic features, and ongoing climate change (Wang and Ding 2021). High PII-CWD values indicate that these regions experience both long precipitation periods and high precipitation intensity during extreme events, increasing the risk of flood disasters.

In contrast, cold spots (indicated in blue) in some areas of NWC and SWC indicate lower intensity of consecutive precipitation events. Drought and low precipitation are the main characteristics of these regions, influenced by terrain, climate zones, and human activities (Cheng *et al.* 2015). Effective mitigation strategies should include improved water resource management, water-efficient agricultural technologies, and ecological restoration initiatives.

The light green areas show relatively uniform distribution of PII-CWD, indicating balanced intensity of extreme precipitation events and relatively stable climate conditions. However, this does not imply that these regions can ignore the impacts of climate change.

Overall, **Figure 9** reveals the risk distribution characteristics of extreme precipitation events across China, with low-risk areas in NWC and NC identified as needing to prioritize drought and water resource management. Future studies should focus on elucidating the mechanistic drivers behind regional variations in PII-CWD under climate change, incorporating socioeconomic dimensions to develop integrated strategies for disaster risk reduction and climate resilience.

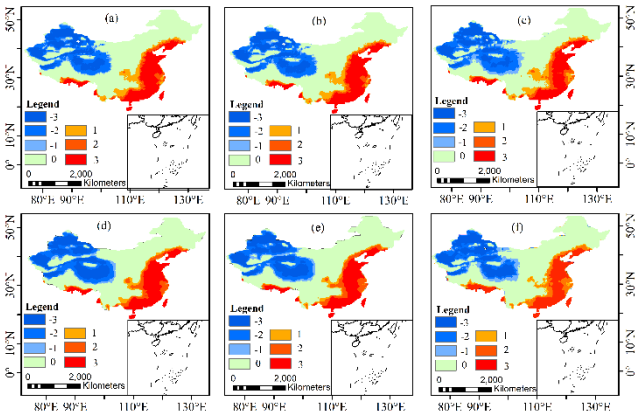

Figure 9. Cluster analysis of PII-CWD under SSP245 and SSP585 scenarios from 2025 to 2100. Panels (a)–(c) show 2025–2050, 2051–2075, and 2076–2100 for SSP245. Panels (d)–(f) show the same periods for SSP585. ±3 represents 99% confidence, ±2 represents 95% confidence, ±1 represents 90% confidence, and 0 indicates no significant difference

5. Conclusions

Based on historical precipitation data and MME precipitation data, this study investigated CWD, TPCWD, PII-CWD, R1, and R2 across China, with the following key findings:

(1) The MME results better reproduce the spatial distribution characteristics of annual average precipitation in China. However, the MME underestimates the annual average precipitation in most regions by over 150 mm, particularly in SC and NWC.

(2) CWD and PII-CWD are longest and strongest in SC and SWC, with PII-CWD exceeding 10 mm/day in CC, SC, and EC, reflecting clear east–west contrasts along the "Hu Huanyong Line".

(3) Future projections show that extreme precipitation intensity (ΔPII-CWD) increases more under SSP585 than SSP245, particularly in SWC, highlighting the stronger impacts of high-emission scenarios.

(4) SC and NC are projected to face notable increases in extreme precipitation events after 2070, while other regions remain relatively stable.

Overall, these results indicate that extreme precipitation events in China will intensify under future climate change, underscoring the urgency of emission reduction and adaptive planning for regional water-related disaster risks.

Funding

This project is supported by the open fund of the Beijing Key Laboratory of Urban Hydrological Cycle and Sponge City Technology（HY2025OF01）; the National Key R&D Plan of China (Grant No.2021YFC3001401); The rainfall trend prediction and the key points discussion of flood prevention in the North China Plain (CZ-2024020). Science Research Project of Hebei Education Department (No.QN2025850).

Author Contributions

Meifang Ren designed the experiments and analyzed the data; Rui Zhang worked on paper and interpreted the results; Fang Yuan revised the manuscript.

Conflicts of Interest

The authors declare no conflicts of interest.

References

Acquaotta, F., Faccini, F., Simona, F., Paliaga, G., Sacchini, A., Vilimek, V. (2019). Increased flash flooding in Genoa Metropolitan Area: a combination of climate changes and soil consumption? Meteorol. Atmos. Phys, 131(2):1-12 https://doi.org/10.1007/s00703-018-0623-4.

Ai, Y., Chen, H., Sun, J. (2022). Model assessments and future projections of spring climate extremes in China based on CMIP6 models. In J Climatol, 42:4601-4620.

Alexander, L.V. (2016). Global observed long-term changes in temperature and precipitation extremes: a review of progress and limitations in IPCC assessments and beyond. Weather Clim. Extrem., 11, 4–16. https://doi.org/10.1016/j.wace.2015.10. 007.

Allan, R.P., Soden, B.J. (2008). Atmospheric warming and the amplification of precipitation extremes. Science, 321: 1481–1483. https://science.sciencemag.org/content/321/5895/1481.

Ávila, Á., Guerrero, F.C., Escobar, Y.C., Justino, F. (2019). Recent Precipitation Trends and Floods in the Colombian Andes. Water, 11, 379. https://doi.org/10.3390/w11020379.

Brown, M., Funk, C. (2008). Food Security under climate Change. Science, 319, 580–581. https://doi.org/10.1126/science.1154102.

Cai, X., Song, Y., Cai, L., Su, X., Liang, G.H., Xu, Y.M. (2024). Analysis on characteristics of extreme precipitation indices and atmospheric circulation in Northern Shanxi. Res Cold Arid Reg, 16: 84-97. https://doi.org/10.1016/j.rcar.2024.03.007.

Cai,W.J., Li, H.R., Lei,M.Y., Cui, X.Q., Sun,F.,Wang,C. (2020). Reality and challenges of China's water resources management in the context of climate change. China's Resources, Energy Sustain. Dev,. Springer, Singapore. https://doi.org/10.1007/978-981-33-6100-3_5.

Chen, H., Sun, J., Lin, W., Xu, H. (2020). Comparison of CMIP6 and CMIP5 models in simulating climate extremes. Sci. Bull., 65(17), 1415–1418.

Chen, X., Yang, T., Shao, Q., Hao, Z., Zhang, Z., Xu, C.Y., Sun, L. (2019). Precipitation extremes in the Yangtze River Basin,

China: regional frequency and spatial–temporal patterns. Theor. Appl. Climatol.,135(1-2), 187-201.

Cheng, A.F., Feng, Q., Wang, G., Cheng, A.F., Feng, Q., Fu, G.B., Zhang, J.K., Li, Z.X., Hu, M., Wang, G.(2015). Recent changes in precipitation extremes in the Heihe River basin, Northwest China. Adv Atmos Sci, 32:1391–1406. https://doi.org/10.1007/s00376-015-4199-3.

Cook, B. I., Ault, T.R.; Smerdon, J.E. (2020). Unprecedented 21st-century drought risk in the American Southwest and Central Plains. Sci. Adv., 6(21), eaaz4571.

Croitoru, A., Piticar, A., Burada, D.C. (2016). Changes in precipitation extremes in Romania. Quat. Int., 415, 325–335. doi.org/10.1016/j.quaint.2015.07.028.

Dong, S.Y., Xu, Y., Zhou, B.T., Shi, Y. (2015). Assessment of indices of temperature extremes simulated by multiple CMIP5 Models over China. Adv. Atmos. Sci., 32(8):1077-1091.

Eyring, V., Cox, P.M., Flato, G.M., Gleckler, P.J., Abramowitz, G., Caldwell, P., Collins, W.D., Gier, B.K., Hall, A.D., Hoffman, F.M., Hurtt, G.C., Jahn, A., Jones, C.D., Klein, S.A., Krasting, J.P., Kwiatkowski, L., Lorenz, R. (2019). Taking climate model evaluation to the next level. Nat. Clim. Change., 9(2), 102-110.

Getis, A., Ord, J.K. (1992). The Analysis of Spatial Association by Use of Distance Statistics. Geogr Anal, 24(3): 189-206. DOI: 10.1111/j.1538-4632.1992.tb00261.x.

Huang, Q., Zhang, Q., Singh, V.P., Shi, P., Zheng, Y. (2017). Variations of dryness/wetness across China: changing properties, drought risks, and causes. Glob. Planet. Chang., 155, 1–12. https://doi.org/10.1016/j.gloplacha.2017.05.010.

IPCC. Climate Change. (2021). The physical science basis. Contribution of working group I to the Sixth assessment report of the intergovernmental panel on climate change. Cambridge: Cambridge University Press.

Ji, Z.M., Kang, S.C. (2015). Evaluation of extreme climate events using a regional climate model for China. Int. J. Climatol., 35 (6): 888-902.

Jiang, D., Hu, D., Tian, Z., Lang, X. (2020). Differences between CMIP6 and CMIP5 models in simulating climate over China and the East Asian monsoon. Adv. Atmos. Sci., 37, 1102–1118.

Jiao, N.Z., Chen, D.K., Luo, Y.M., Huang, X.P., Zhang, R., Zhang, H.B., Jiang, Z.J., Zhang, F. (2015). Climate change and anthropogenic impacts on marine ecosystems and counter measures in China. Adv. Clim. Chang. Res., 6, 118–125.https://doi.org/10. 1016/j.accre.2015.09.010.

Kharin, V.V., Zwiers, F.W., Zhang, X., Wehner, M. (2013). Changes in temperature and precipitation extremes in the CMIP5 ensemble. Clim. Change.,119(2), 345-357.

Kumar, P., Kumar, S., Barat, A., Sarthi, P.P., Sinha, A.K. (2020). Evaluation of NASA's NEX-GDDP-simulated summer monsoon rainfall over homogeneous monsoon regions of India. Theor. Appl. Climatol., 141, 525–536.

Li, K.Z., Wu, S.H., Dai, E.F., Xu, Z.C. (2012). Flood loss analysis and quantitative risk assessment in China. Nat. Hazards, 63, 737–760. https://doi.org/10.1007/s11069-012-0180-y.

Li, L.C., Yao, N., Liu, D.L., Song, S.B., Lin, H.X., Chen, X.G., Li,Y. (2019). Historical and future projected frequency of extreme precipitation indicators using the optimized cumulative distribution functions in China. J Hydrol., 579:124170.

Li, Z., Li, Y.P., Shi, X.P., Li, J.J. (2017). The characteristics of wet and dry spells for the diverse climate in China. Glob. Planet. Chang., 149, 14–19. https://doi.org/10.1016/j. gloplacha.2016.12.015.

Lin, L., Wang, Z., Xu, Y., Fu, Q. (2018). Sensitivity of precipitation extremes to radiative forcing of greenhouse gases and aerosols. Geophys. Res. Lett., 45(14), 7857-7865.

Lun, Y., Liu, L., Cheng, L., Li, X.P., Li, H., Xu, Z.X. (2021). Assessment of GCMs simulation performance for precipitation and temperature from CMIP5 to CMIP6 over the Tibetan Plateau. Int. J. Climatol,41(7):3994-4018.

Ma, Z., Sun, P., Zhang, Q., Zou, Y.F., Lv, Y.F., Li, H., Chen, D.H. (2022). The characteristics and evaluation of future droughts across China through the CMIP6 multi-Model ensemble. Remote. Sens-Basel, 14(5): 1097.

Mandelbrot, B.B., Wallis, J.R. (1968). Joah, Joseph, and operational hydrology. Water Resour Res., 4(5), 909-918.

Mishra, A.K., Singh, V.P., Jain, S.K. (2010). Impact of global warming and climate change on social development. J. Comp. Soc. Welfare, 26, 239–260. https://doi.org/10.1080/17486831003687626.

O'Neill, B.C., Kriegler, E., Riahi, K., Kristie, L., Stephane, H., Timothy, R., Ritu, M., Detlef, P.V. (2014). A new scenario framework for climate change research: the concept of shared socioeconomic pathways. Clim. Change, 122, 387–400.

Papalexiou, S.M., Montanari, A. (2019). Global and regional increase of precipitation extremes under global warming. Water Resour. Res., 55, 4901–4914. https://doi.org/10.1029/2018WR024067.

Peng, L., Yi, L., Hao, F. (2017). The best alternative for estimating reference crop evapo-transpiration in different sub-regions of mainland China. Sci. Rep., 7 (1), 5458.

Riahi, K., Vuuren, D.P., Tavoni, M., Kriegler, E., Edmonds, J., O'Neill, B.C., Fujimori, S., Bauer, N., Calvin, K., Dellink, R., Fricko, O., Lutz, W., Popp, A., Cuaresma, J.C., KC, S., Leimbach, M., Jiang, L., Kram, T. (2017). The Shared Socioeconomic Pathways and their energy, land use, and greenhouse gas emissions implications: An overview. Glob. Environ. Change., 42: 153-168. DOI:10.1016/j.gloenvcha.2016.05.009.

Roque-Malo, S., Kumar, P. (2017). Patterns of change in high frequency precipitation variability over North America. Sci. Rep., 7, 10853. https://doi.org/10.1038/s41598-017-10827-8.

Sheffield, J., Justin, Goteti, Gopi, Wood E., Eric, F. (2006). Development of a 50-year high-resolution global dataset of meteorological forcings for land surface modeling. J. Clim., 19, 3088.

Shi, J., Cui, L., Wen, K., Tian, Z., Wei, P., Zhang, B. (2018). Trends in the consecutive days of temperature and precipitation extremes in China during 1961–2015. Environ. Res.,161, 381–391. https://doi.org/10.1016/j.envres.2017.11.037.

Shruti, V., Bhatla, R. (2020). Performance of RegCM4 for Dynamically Downscaling of El Nino/La Nina Events During Southwest Monsoon Over India and Its Regions. Earth. Space. Sci., 8.e2020EA001474. https://doi.org/10.1029/2020EA001474.

Singh, D., Tsiang, M., Rajaratnam, B., Diffenbaugh, N.S.(2014). Observed changes in extreme wet and dry spells during the south Asian summer monsoon season. Nat. Clim. Chang., 4, 456–461. https://www.nature.com/articles/nclimate2208.

Sura, P. (2011). A general perspective of extreme events in weather and climate. Atmos. Res., 101, 1–21. https://doi.org/10.1016/j.atmosres.2011.01.012.

Tammets, T., Jaagus, J. (2013). Climatology of precipitation extremes in Estonia using the method of moving

precipitation totals. Theor. Appl. Climatol., 111, 623–639. https:// doi.org/10.1007/s00704-012-0691-1.

Thrasher, B., Wang, W., Michaelis, A., Melton, F., Lee, T., Nemani, R. (2022). NASA global daily downscaled projections, CMIP6. Sci.Data, 9, 262.

Tian,J.X., Zhang,Z.X., Ahmed, Z., Zhang,L.Y., Su, B.D., Tao,H., Jiang,T. (2021). Projections of precipitation over China based on CMIP6 models. Stoch. Environ. Res. Risk Assess., 35:831-838.

Wang, B., Ding, Q.H. (2021). Changes in global monsoon precipitation over the past 56 years. B Am Meteorol Soc, 102(1):1-19.

Wu, F., Jiao, D.L., Yang, X.L., Cui, Z.Y., Zhang, H.S., Wang, Y.H. (2023). Evaluation of NEX-GDDP-CMIP6 in simulation performance and drought capture utility over China - based on DISO. Hydrol. Res., 54 (5): 703.

Wu, J.F., Chen, X.H. (2019). Spatiotemporal trends of dryness/wetness duration and severity: the respective contribution of precipitation and temperature. Atmos. Res, 216, 176–185. https://doi.org/10.1016/j.atmosres. 2018.10.005.

Xiang, J., Zhang, L., Deng, Y. (2021). Projection and evaluation of extreme temperature and precipitation in major regions of China by CMIP6 models. Engineering Journal of Wuhan university, 54(1): 46-57, 81.

Yang, X.L., Zhou, B.T., Xu, Y., Han, Z.Y. (2021). CMIP6 evaluation and projection of temperature and precipitation over China. Adv. Atmos. Sci.,38, 817–830. https://doi.org/10.1007/ s00376-021-0351-4.

Yang, Y., Tang, J.P., Liu, G., Yang, Y., Tang, J.P., Wang, S.Y. (2018). Differential impacts of 1.5 and 2°C warming on extreme events over China using statistically downscaled and bias-corrected CESM low-warming experiment. Geophys. Res. Lett., 45 (18): 9852-9860.

Yuan, Z., Yang, Z.Y., Yan, D.H., Yin, J. (2017). Historical changes and future projection of extreme precipitation in China. Theor. Appl. Climato., 127(1-2) :393-407. doi: 10. 1007 /s00704-015-1643-3.

Zeng, S., Liu, Z., Kaufmann, G. (2019). Sensitivity of the global carbonate weathering carbonsink flux to climate and land-use changes. Nat. Commun., 10, 5749.

Zhan, Y., Ren, G., Arun, B.S., Rupak, R., Ren, Y.Y., Jayanarayanan, S., Xu, Y., Sun, X., You, Q.L., Wang, S. (2017). Changes in extreme precipitation events over the Hindu Kush Himalayan region during 1961–2012. Adv. Clim. Chang. Res., 8, 166–175. https://doi.org/10.1016/j.accre.2017.08.002.

Zhang, Q., Liu, C.L., Xu, C.Y., Xu, Y.P., Jiang, T. (2008). Spatial and temporal variability of precipitation maxima during 1960–2005 in the Yangtze River basin and possible association with large-scale circulation. J. Hydrol., 353(3-4), 215-227.

Zhang, Y., Hu, X., Zhang, Z., Xiao, M.Z., Singh, V.P., Leung, Y., Jiang, L.G. (2023). The increasing risk of future simultaneous droughts over the Yangtze River basin based on CMIP6 models. Stoch. Environ. Res. Risk Assess., 37, 2577–2601. https://doi.org/10.1007/s00477-023-02406-3.

Zhang, Y., You, Q., Mao, G., Chen, C., Ye, Z. (2019). Short-term concurrent drought and heatwave frequency with 1.5 and 2.0 C global warming in humid subtropical basins: a case study in the Gan River Basin, China. Clim. Dyn., 52, 4621–4641.

Zhang, Y.Q., You, Q.L., Chen, C.C., Wang, H.J., Ullah, S., Shen, L.C. (2024). Characteristics of flash droughts and their association with compound meteorological extremes in China: Observations and model simulations. Sci. Total Environ.,916:170133. https://doi.org/10.1016/ j. scitotenv. 2024.170133.